Bioinspired snapping-claw apparatus to study hydrodynamic cavitation effects on the corrosion of metallic samples

F. A. Godínez,[1] R. Mayén-Mondragón,[2] J.E.V. Guzmán,[3] O. Chávez,[4] M. Gavaises,[5] and R. Montoya[2, a)]
[1)] *Instituto de Ingeniería, Polo Universitario de Tecnología Avanzada, Universidad Nacional Autónoma de México, Apodaca,N.L., 66629, México.*
[2)] *Facultad de Química, Polo Universitario de Tecnología Avanzada, Universidad Nacional Autónoma de México, Apodaca,N.L., 66629, México.*
[3)] *Instituto de Ingeniería, Universidad Nacional Autónoma de México, Ciudad de México, 04510, México*
[4)] *Tecnológico Nacional de México/I.T. Chihuahua, Chihuahua, Chih., 31310, México.*
[5)] *School of Mathematics, Computer Science & Engineering, City University London, London,EC1V 0HB, UK*

(Dated: 15 April 2020)

A creative low-cost and compact mechanical device that mimics the rapid closure of the pistol shrimp claw was used to conduct electrochemical experiments, in order to study the effects of hydrodynamic cavitation on the corrosion of aluminum and steel samples. Current-time curves show significant changes associated with local variations in dissolved O_2 concentration, cavitation-induced erosion and changes in the nature of the surface corrosion products.

PACS numbers: 07.10.h, 47.27.i, 47.55.dp, 47.70.Fw, 82.45.Fk
Keywords: hydrodynamic cavitation, venturi tube, erosion-corrosion, snapping shrimp

Multiphase-flow piping systems in the oil, gas and nuclear power industries can be exposed to high levels of corrosion and/or erosion resulting in wall thinning and eventually ductile failure and rupture[1]. Thus, understanding the combined effects of corrosion and erosion on diverse piping materials is imperative to reduce equipment replacement costs, production losses, and environmental risks. Different methods to study flow accelerated corrosion using expensive loops and corrosion sensors are found in the specialized literature[2]. The current work presents however an alternative low-space, low-cost technique to detect/measure the synergistic effects of erosion and corrosion on metallic materials. It is based on a recently built and tested mechanical device inspired by the snapper claw of alpheid shrimps[3]. Such claw allows them to produce a high speed cavitating water jet accompanied by shock waves and the emission of short bursts of light[4,5]. The proposed device consists of an upper pivoting claw, a lower claw that is fixed between two parallel walls to form a socket, a set of rubber bands to achieve the rapid closure of the upper claw, and a mechanical trigger to activate the closing process. Figure 1(a) illustrates the main components of this apparatus. Figure 1(b) shows the rectangular venturi-like shape that forms when the total closure of the upper claw is achieved. The device works when immersed in a liquid, while the upper claw is fully open the liquid fills the socket. Then, as the claw closes speedily, the liquid from the socket volume is displaced leading to a jet ($\sim$ 5 m/s) through the venturi opening. In addition to the turbulent (Re $\sim$ 5000) flow jet, the development of various cavitation structures (inside and outside of the tube) have been revealed using high-speed videography[3]. In Ref.[3] it was pointed out that our apparatus allows testing the cavitation regimes produced under different venturi geometries, without the need of utilizing great liquid volumes and typical hydraulic circuits that demand space and expensive equipment such as pumps, pipes, tanks, etc. In fact, it should be noted that there is no limitation to the geometry of the tube and its cross-section. Furthermore, by mounting different metallic samples on the lower claw, their electrochemical response to the turbulent cavitation flow induced by the snapping upper claw can be measured.

The apparatus was set inside a rectangular tank (44 cm $\times$ 44 cm $\times$ 22 cm). A Bio-Logic SP-150 potentiostat was used to follow the electrochemical behavior of two different electrochemical cells (one carbon-steel based, Fig. 1 (c) and the other aluminum-foil based, Fig.1 (d)). All experiments were conducted at room conditions of pressure and temperature (101860 Pa and 23 °C). Figure 2 shows a high-speed photographic sequence revealing cavitating flows inside the tube, with a subsequent series of collapses/expansions of the bubble clouds and clusters in different regions, including the location of the electrochemical cells.
For the carbon-steel cell, a 2 mm diameter carbon-steel rod, serving as a working-electrode (WE), and a 0.5 mm diameter platinum-wire (Sigma-Aldrich) counter-electrode (CE), were inserted into the device lower claw. A silver/silver chloride reference-electrode, RE (Sigma-Aldrich), was placed adjacent to the lower claw. The electric connections were covered with a water proof seal made with epoxy resin. The tank was filled with a 0.005 molar sodium chloride solution. Cathodic polarization and anodic polarization tests were perfomed by applying an overpotential step of -0.25 V and +0.25 V, respectively, between WE and RE. The electric current flow between WE and CE was measured as a function of time. Several seconds after the decay of the initial spike (caused

[a)] Electronic mail: rmontoyal@unam.mx

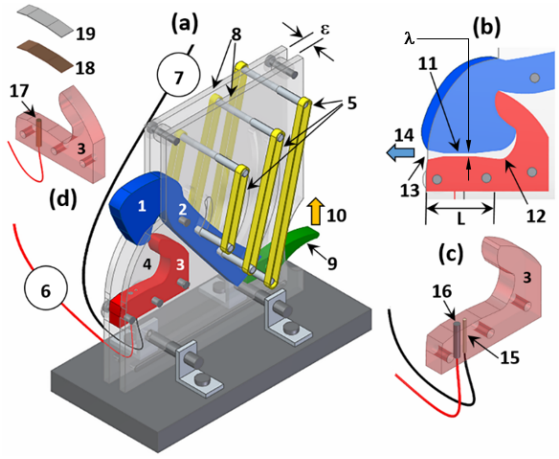

FIG. 1. (a) 3D CAD model of the snapping-claw apparatus to generate transient cavitation (open position): 1) pivoting upper claw, 2) pivot, 3) fixed lower claw, 4) socket, 5) rubber bands, 6) working electrode (WE) connection cable, 7) counter electrode (CE) connection cable, 8) parallel support walls separated by distance ϵ= 5.8 mm, 9) mechanical trigger, 10) trigger activation direction. (b) venturi geometry, 11) throat section, 12) closed end, 13) open end, 14) liquid jet direction. Length of the venturi L = 22.31 mm. Characteristic length at the venturi neck $\lambda = 1$ mm, thus the Reynolds number is defined as $\mathrm{Re} = u \cdot \lambda \cdot \rho/\mu$. (c) Lower fixed claw with (15) platinum rod as CE and (16) steel rod as WE. (d) Lower fixed claw with (17) copper rod, (18) copper foil as connection elements and (19) aluminum foil as WE.

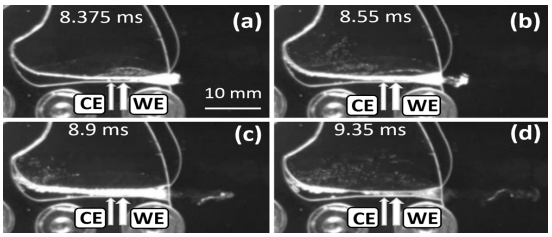

FIG. 2. A high-speed cross section photographic sequence of the cavitation during the final stages of the device closure. All frames were captured with a Phantom v1212 camera at 40,000 fps and exposure time of 10 μs. The white arrows indicate the location of WE and CE. (a) The formation of a single vapor lobe and the emergence of a thin bubble layer on the upper contour of the venturi (8.375 ms is the time that has elapsed since the upper claw is released). (b) The bubble layer grows in thickness, and a vortex ring is detached from the single lobe. (c) The bubble layer becomes thicker, filling entirely the throat as well as other sections of the venturi; meanwhile, the vortex collapses and expands every time with less intensity. (d) Rapid collapses and expansions of the bubble clusters inside the venturi.

by the potential step applied at t = 0 s), the closure of the biomimetic device was triggered. Afterwards, the WE surface was polished with silicon carbide paper to conduct the following fifteen tests under anodic polarization. A carbon-steel reference sample was immersed inside the tank in a region with very low turbulent effects. Optical-microscope images of the WE and reference sample surfaces were taken before and after each set of tests.

For the aluminum cell, an aluminum foil (0.75 cm^2) WE was attached on the lower-claw surface. Both, the CE and RE were located adjacent to the lower claw. The WE area used in this cell allowed integrating a larger number of cavitation events into the electrochemical signal. Open circuit potential (OCP) and anodic polarization tests were performed for this cell configuration. During the former, the closure process of the device was triggered several consecutive times. For the latter, an overpotential step of +0.20 V was applied between WE and RE.

Figure 3(a), curve (1), shows the typical current-time response registered during the cathodic polarization tests with the carbon-steel cell. The electrochemical reduction of dissolved oxygen at the electrode surface generates a negative current. The current spike at t = 0 s results from the reduction of an initially large amount of oxygen adjacent to the electrode surface. Afterwards, the current reaches a steady state value where the rate of oxygen mass-transport from the water bulk to the electrode surface, equals the rate of gas reacting at the same location. At around t = 4.19 s, the snapping process takes place. The sudden large current increase (negatively, see Fig. 3(a) inset) can be explained by the turbulent transport of reacting oxygen to the electrode surface. Around 20 ms later, the flow related effects are reduced and the current attains a second stationary value. Therefore, when hydrodynamic cavitation erodes the metallic surface, a higher current-stationary-value is achieved (see Fig. 3(a), curve (2)). This is due to the resulting increase in the electrode surface area.

Figure 3(b) shows the typical current-time response registered during the anodic polarization tests on the carbon-steel sample. The electrochemical oxidation of the electrode generates the positive-current flow. As in the cathodic polarization case, the current attains a steady state value after the initial spike at t = 0 s. Upon the closure of the device, at around 3.7 s, a sudden large current decrease is registered. The oxygen supplied to the electrode surface promoted by the cavitating flow favors the formation of corrosion products with a higher oxygen content. For the steel case, such products are more resistant to the diffusion of oxygen towards the metallic surface, thus reducing the corrosion rate to a very low value[6,7]. Once the fluid flow is stabilized, transformation to the corrosion products with a lower oxygen content (enforced by thermodynamic equilibrium) modulates the current reaching a steady state. This inhibition effect is opposite to what occurs with other metals, for which the combination of flow and increased oxygen supply accelerates the corrosion process (flow-accelerated corrosion).

Figure 3(c) compares the WE and reference sample surfaces after the cathodic polarization runs. A series of pits within a large crater are observed in the former electrode, Fig. 3(c)(1). The erosion caused by the sequence of cavitation tests seems to reveal regions with higher susceptibility to the attack of chloride ions. The reference sample shows only minor damage (Fig. 3(c)(2)).

Figure 4(a) shows the OCP evolution during four consecutive claw snapping events using the aluminum foil sample. Each time the upper-claw is closed, the metallic surface becomes more active recovering its natural elec-

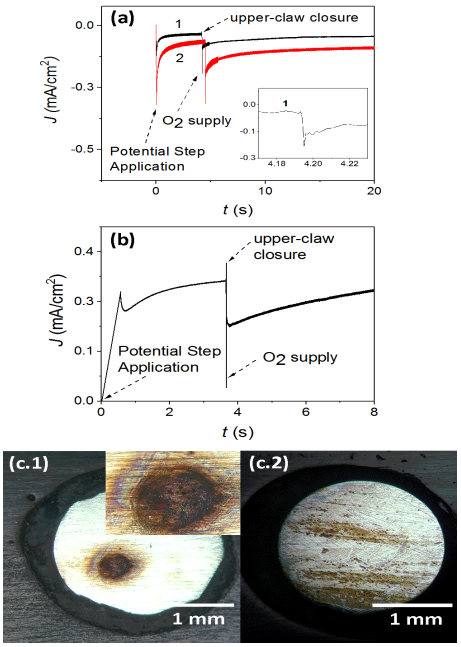

FIG. 3. (a) Current-time response of the carbon steel sample (cathodic polarization at -0.25 V vs. OCP) during hydrodynamic cavitation produced by the mechanical device. (1) Typical response; (2) response associated to cavitation-induced erosion. Inset: zoom in around 4.20 s when the claw is closed. (b) Current-time response of the carbon steel sample (anodic polarization at +0.25 V vs. OCP) during hydrodynamic cavitation produced by the mechanical device.(c) Optical-microscope images of the metallic surface after the cathodic polarization runs. (1) WE; (2) reference sample.

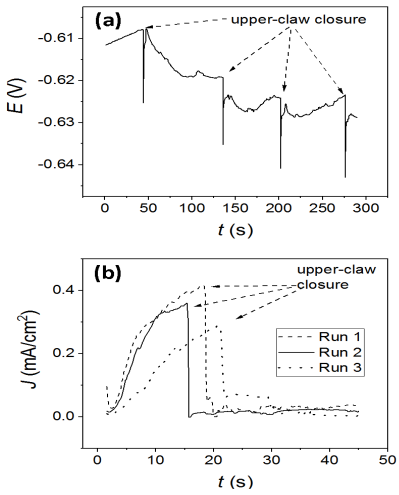

FIG. 4. (a) OCP of the aluminum foil showing acute drops during the activation of the mechanical device. (b) Current-time curve of the aluminum sample (anodic polarization at +0.20 V vs. OCP) showing how the current density drops down due to the hydrodynamic cavitation.

trochemical behaviour after a couple of seconds. This indicates that a fresh electrode surface is exposed to the electrolyte once the mechanical device is activated. When a metal is in contact with an electrolyte, the surface starts corroding from the very beginning and two kinds of corroded films are expected, depending on the material and the electrolyte: a hard, fragile and easily removable film, and a compact film strongly bounded to the metallic surface[8]. Aluminum produces a film of compact corrosion products. The results plotted in Fig 4(a) confirm that the hydrodynamic conditions generated during the snapping event break the products film in a tiny area exposing a fresh metallic surface to the electrolyte. This surface is clearly detected by the electrochemical cell mounted on the system. The recovery of the potential (after few seconds) indicates that the corrosion products film has been regenerated in the tiny damaged zone. Figure 4(b) shows the current-time response registered during three anodic polarization runs. A large current-drop caused by the closure process can be observed. Under anodic polarization, once the aluminum dissolution starts, a porous oxide layer is generated. Nevertheless, before a steady state is attained, there is a noisy stage where many aluminum compounds are formed and the current fluctuates[9]. Therefore, when the mechanical device is activated a fresh metallic surface is revealed to the electrolyte and the new chemical environment produces electrical perturbations. The current is significantly decreased and a longer period of time is then necessary to recover the characteristic steady state current signal[10].

In summary, the designed biomimetic device allows one to study, in a compact and economical way, the effects of a turbulent fluid flow on the cavitation-induced corrosion-erosion processes on metallic surfaces. It can also be used to test flow-subjected non-metallic surfaces, for example, to evaluate the resistance of anticorrosive coatings[11]. The device can be particularly helpful to follow the behavior of mass-transport-limited electrochemical-processes under high-Reynolds flow-regimes. Additionally, this device is able to reproduce pressure changes in venturi systems (and other geometries) simplifying complex pipeline arrangements. On the other hand, the equipment, by using electrochemical techniques, allows predicting the lifespan of metallic pipeline systems. We are currently working to automate the system controlling the closure frequency of the device. The goal is to study the influence of selected experimental parameters on the flow-accelerated corrosion of metallic samples.

We wish to acknowledge financial support from the DGAPA-PAPIIT (UNAM) grant TA100119 and valuable scientific discussions with Prof. J. Genesca.

[1]V. Kain, Procedia Engineering **86**, 576 (2014).
[2]Y. Utanohara, K. Kamahori, A. Nakamura, and M. Murase, E-Journal of Advanced Maintenance **8**, 1 (2016).
[3]F. A. Godínez, M. Navarrete, O. Chávez, and E. Guzmán, in *Proceedings of the 10th International Symposium on Cavitation (CAV2018)*, edited by J. Katz (ASME Press, Baltimore, 2018).
[4]D. Lohse, B. Schmitz, and M. Versluis, Nature **413**, 477 (2001).
[5]P. Koukouvinis, C. Bruecker, and M. Gavaises, Sci. Rep.-UK **7**, 1 (2017).
[6]H. Forrest, B. E. Roetheli, and R. Brown, Ind. Eng. Chem **23**, 650 (1931).
[7]G. Cox and B. Roetheli, Ind. Eng. Chem **23**, 1012 (1931).
[8]Y. Waseda, S. Suzuki, and Y. Waseda, *Characterization of corrosion products on steel surfaces*, Vol. 1 (Springer, 2006).
[9]V. Troutner, Corrosion **15**, 25 (1959).

[10]The data that support the findings of this study are available from the corresponding author upon reasonable request.

[11]P. A. Sørensen, S. Kiil, K. Dam-Johansen, and C. E. Weinell, Journal of Coatings Technology and Research **6**, 135 (2009).